

EFFECTS OF FLYING WING CONFIGURATION PARAMETERS ON AERODYNAMICS AND STABILITY

Yuxing Gao [1], Huan Zhao [2], Keyao Gan [3]

[1-3] School of Aeronautics, Northwestern Polytechnical University, Xi'an, Shaanxi, 710072, China

Abstract

A representative flying-wing baseline configuration is investigated to quantify how three planform parameters influence aerodynamic efficiency and stability under a constant projected area of 280.34 m². The aspect ratio and the leading- and trailing-edge sweep angles are varied within representative ranges, and the resulting trends are evaluated using steady viscous computations for lift, drag and static stability, complemented by a limited set of unsteady forced-oscillation computations for damping characteristics at Mach 0.2. For aerodynamic performance, the lift-to-drag ratio typically reaches its peak at α = 4°-6° at Mach 0.2, while the sensitivity to leading-edge sweep is modest in the low-speed regime but becomes more pronounced at Mach 0.8 due to compressibility effects. For static stability, both Mach 0.2 and Mach 0.8 results indicate that increasing aspect ratio tends to reduce longitudinal static stability, whereas a larger leading-edge sweep angle and an intermediate trailing-edge sweep angle promote a more favorable pitching-moment trend in the small-angle range. For dynamic stability at Mach 0.2, the trailing-edge sweep angle shows the strongest impact on pitch and roll damping at zero angle of attack, and the pitch damping sensitivity increases beyond an angle of attack of about 6°. These findings establish a practical early-stage screening logic: use aerodynamic efficiency to identify candidate configurations, enforce static-stability constraints through sweep selection, and finally prioritize trailing-edge sweep for damping robustness in the low-speed flight regime.

Keywords: Flying wing; CFD; Configuration parameters; Static stability; Damping derivatives

1 Introduction

Flying-wing and blended-wing-body configurations have long been recognized as promising candidates for improved aerodynamic efficiency, yet their tailless nature makes stability and control constraints an integral part of early-stage design. Mader and Martins [1] demonstrated that enforcing stability constraints can substantially alter the feasible design space in flying-wing aerodynamic optimization, underscoring the need to treat performance and stability in a coupled manner. In a related context, Lyu and Martins [2] performed aerodynamic design optimization for a blended-wing-body aircraft and highlighted the importance of planform shaping in achieving efficiency gains. From a stability-and-control perspective, Park et al. [3] studied tailless aircraft using a variable-fidelity aerodynamic analysis framework, emphasizing that credible stability assessment often requires a careful balance between model fidelity and computational cost. Earlier foundational work compiled in classic NACA reports [4] also summarized stability and control challenges specific to tailless airplanes, providing qualitative guidance that remains useful for modern configurations. Standard definitions and interpretation of static and dynamic stability metrics commonly follow canonical flight-dynamics references such as Etkin and Reid [5].

Beyond static stability, dynamic stability derivatives are essential for assessing damping characteristics and dynamic robustness, yet their acquisition is substantially more demanding. CFD-based approaches have been widely explored to compute dynamic derivatives via prescribed periodic motions. Da Ronch et al. [6] discussed the computation of dynamic derivatives for full aircraft configurations using Euler/RANS methods with forced periodic motions, and later Da Ronch et al. [7] evaluated the

formulation and practical accuracy of CFD-derived dynamic derivatives in unsteady aerodynamic contexts. For experimental and hybrid methodologies, forced-oscillation testing remains a cornerstone, and Vicroy [8] provided a detailed guide for forced-oscillation data processing and analysis, including practical procedures for amplitude–phase extraction and derivative identification. More recently, frequency-domain techniques that transform unsteady CFD responses into harmonic components have been proposed as a systematic pathway for derivative estimation; Nguyen et al. [9] presented a frequency-domain method based on unsteady RANS simulations and Fourier-series processing.

Despite these advances, existing studies often emphasize either aerodynamic optimization or stability assessment in isolation, while a compact "planform-parameter–performance–stability" sensitivity chain suitable for early-stage screening remains comparatively less documented, especially when both static trends (over a practical angle-of-attack range) and selected dynamic-derivative baselines are required under consistent geometric constraints. Motivated by this gap, the present work performs a controlled planform-parameter study for a representative flying-wing configuration at constant projected area, quantifies aerodynamic efficiency and static stability trends using steady viscous simulations at Mach 0.2 and Mach 0.8, and complements them with a limited yet informative set of unsteady forced-oscillation computations at Mach 0.2 to assess damping-derivative sensitivity.

2 Configuration Parameterisation and Analysis Methods

2.1 Baseline configuration and planform parameters

A single-sweep flying-wing configuration is selected as the baseline configuration in this study. The main objective is to investigate how the planform parameters of this flying-wing layout influence aerodynamic performance, static stability, and damping derivatives. To ensure consistency among different variants, all planform variants are constrained to have the same projected planform area, with a reference area of S = 280.34 m^2.

Three representative planform parameters are considered in a one-factor-at-a-time manner: aspect ratio AR, leading-edge sweep angle Λ_{LE}, and trailing-edge sweep angle Λ_{TE}. For the aspect-ratio family, the leading- and trailing-edge sweep angles are kept unchanged, and the tested aspect ratios are AR = 3.902, 5.255, and 6.960. The wing span and chord-length distribution are adjusted to satisfy the prescribed AR under the constant-area constraint. For the leading-edge sweep family, the trailing-edge sweep angle is fixed at 35°, and the tested leading-edge sweep angles are Λ_{LE} = 35°, 37°, and 39°, while both the projected planform area and the wing span are kept constant. For the trailing-edge sweep family, the leading-edge sweep angle is fixed at 35°, and the tested trailing-edge sweep angles are Λ_{TE} = 35°,37°, and 39°, while the projected planform area and wing span are also kept constant.

This parameterisation strategy allows the effects of AR, Λ_{LE}, and Λ_{TE} to be examined under controlled geometric constraints. In particular, the constant-area constraint avoids a direct comparison between configurations with different reference areas, while the constant-span setting in the sweep-angle studies reduces the influence of overall size variation on the aerodynamic and stability trends. The definitions of the planform parameters are shown in Figure 1. The main symbols, parameter levels, flight conditions, output metrics, and grid settings are summarized in Table 1.

Table 1 - Nomenclature, parametric variations and computational conditions used in this study.

Category	Item	Definition / Setting
Geometry & parameters	S	Projected planform area, held constant at 280.34 m²
	b	Wing span
	AR	Aspect ratio, AR = b²/S; levels: 3.902, 5.255, 6.960
	Λ_{LE}	Leading-edge sweep; levels: 35°, 37°, 39°
	Λ_{TE}	Trailing-edge sweep; levels: 35°, 37°, 39°
Flight conditions	M	Mach number: 0.2 and 0.8
	α	Angle of attack:

Category	Item	Definition / Setting
Output metrics	β	Sideslip angle used for lateral-directional static stability assessment
	C_L, C_D	Lift and drag coefficients
	L/D	Lift-to-drag ratio
	$C_m(\alpha)$	Pitching-moment coefficient vs. angle of attack
	$C_l(\beta)$,$C_n(\beta)$	Roll/yaw stability derivatives vs. sideslip
	C_{mq}, C_{lp}, C_{nr}	Pitch/roll/yaw damping derivatives
CFD setup	Δy_1	First-layer wall-normal height for both grids: 1×10^{-5} m
	ΔS_{surf}	Structured surface grid size: min 0.005 m, max 0.2 m
	L_{edge}	Unstructured surface mesh edge length: min 0.00347 m, max 0.438 m

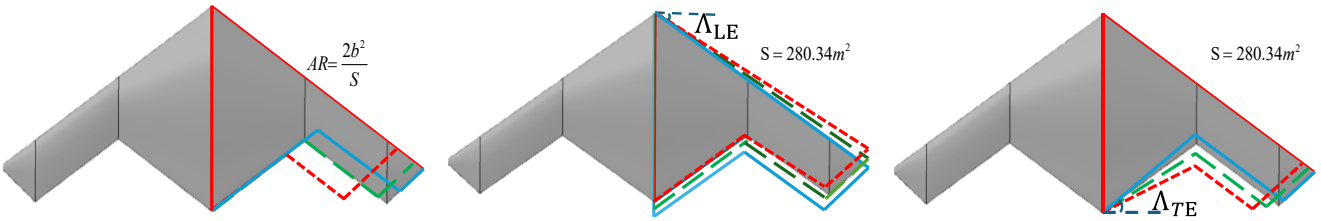


Figure 1 - Planform parameter definition for AR, Λ_{LE} and Λ_{TE} (schematic).

2.2 Steady RANS analysis for aerodynamic performance and static stability

Steady aerodynamic and static-stability computations were performed using CFL3D [10] on structured multi-block grids. The Reynolds-averaged Navier–Stokes equations were solved with the Spalart–Allmaras turbulence model. To ensure a consistent comparison among different planform variants, the same solver settings, grid-generation strategy, boundary-condition definitions, and moment reference point were used for all cases. The moment reference point was located at 25% of the mean aerodynamic chord, measured from the leading edge in the streamwise direction.

Two Mach numbers were considered, namely M = 0.2 and M = 0.8. The low-speed condition was used to evaluate the basic aerodynamic performance and static-stability characteristics of the flying-wing layout, while the higher-Mach-number condition was included to examine the influence of compressibility on the planform-parameter trends. For M = 0.2, the angle of attack was varied from −5° to 20° with an increment of 2°. For M = 0.8, the angle of attack was varied from −5° to 15° with the same increment. For lateral-directional static-stability assessment, the sideslip angle was varied from −5° to 5° with an increment of 1°.

The aerodynamic performance was evaluated using the lift coefficient C_L, drag coefficient C_D, and lift-to-drag ratio L/D. Longitudinal static stability was assessed from the variation of the pitching-momen t coefficient C_m with angle of attack α. In the small-angle range, the sign and magnitude of $C_{m\alpha}$ were used to indicate the longitudinal restoring tendency, with a more negative $C_{m\alpha}$ corresponding to a str onger longitudinal static-stability tendency. Lateral-directional static stability was evaluated from the variations of the rolling-moment coefficient C_l and yawing-moment coefficient C_n with sideslip angle β, with particular attention paid to the near-zero-sideslip trends of $C_{l\beta}$ and $C_{n\beta}$.

The full-span structured grid contained approximately 6.7 million cells, as checked using Tecplot. The first-layer wall-normal height was 1×10^{-5} m, and the characteristic surface grid size ranged from 0.005 m to 0.2 m. A case was considered converged when the residuals decreased to the order of 10^{-6} and the aerodynamic force and moment coefficients varied only within a small range over the final iterations.

2.3 Forced-oscillation analysis for damping-derivative extraction

In addition to the steady CFL3D computations, unsteady forced-oscillation simulations were performed in ANSYS Fluent to extract the damping derivatives of the flying-wing layout. The prescribed rigid-body harmonic motions were imposed through user-defined functions, and the unsteady aerodynamic moment histories exported from Fluent were post-processed using MATLAB. Since forced-oscillation computations require multiple unsteady cycles and are considerably more expensive than steady computations, the dynamic-stability analysis was limited to M = 0.2.

The unsteady computations were conducted on unstructured grids. The same first-layer wall-normal height of 1×10^{-5} m was used, and the surface mesh edge length ranged from 0.00347 m to 0.438 m. The free-stream velocity was 68.0 m/s, corresponding to the low-speed Mach number considered in this study.

For each forced-oscillation case, a small-amplitude harmonic angular motion was prescribed about the corresponding body axis. The general form of the imposed motion is given by Eq. (1).

$$\theta(t) = \theta_0 + A\sin(\omega t) \tag{1}$$

where θ denotes the pitch, roll, or yaw motion variable, θ_0 is the mean attitude angle, A is the oscillation amplitude, and ω is the angular frequency. In the present computations, $\theta_0 = 0°, A = 0.5°$, and $\omega = 7.44$ rad/s. The corresponding period is approximately 0.845 s.

Three principal damping derivatives were extracted at α = 0° and β = 0°, including the pitch damping derivative C_{mq}, the roll damping derivative C_{lp}, and yaw damping derivative C_{nr}. In addition, pitch damping was further evaluated over α = 0° to 10° to examine the sensitivity of C_{mq} to angle of attack.

During the derivative extraction, the initial transient response was first removed, and the aerodynamic moment histories in the periodic response stage were then fitted using a least-squares procedure. For pitch oscillation, the pitching-moment coefficient was fitted as a function of angle of attack and the non-dimensional pitch rate $\hat{q} = q\bar{c}/(2V_\infty)$. For roll and yaw oscillations, the rolling- and yawing-moment coefficients were fitted using sideslip angle and the corresponding non-dimensional angular rates $\hat{p} = pb/(2V_\infty)$ and $\hat{r} = rb/(2V_\infty)$, respectively.

The overall computational procedure of the present study is summarized in Figure 2.s The analysis is organized progressively from planform parameterisation to steady aerodynamic/static-stability evaluation and then to unsteady damping-derivative extraction, supporting early-stage flying-wing configuration screening.

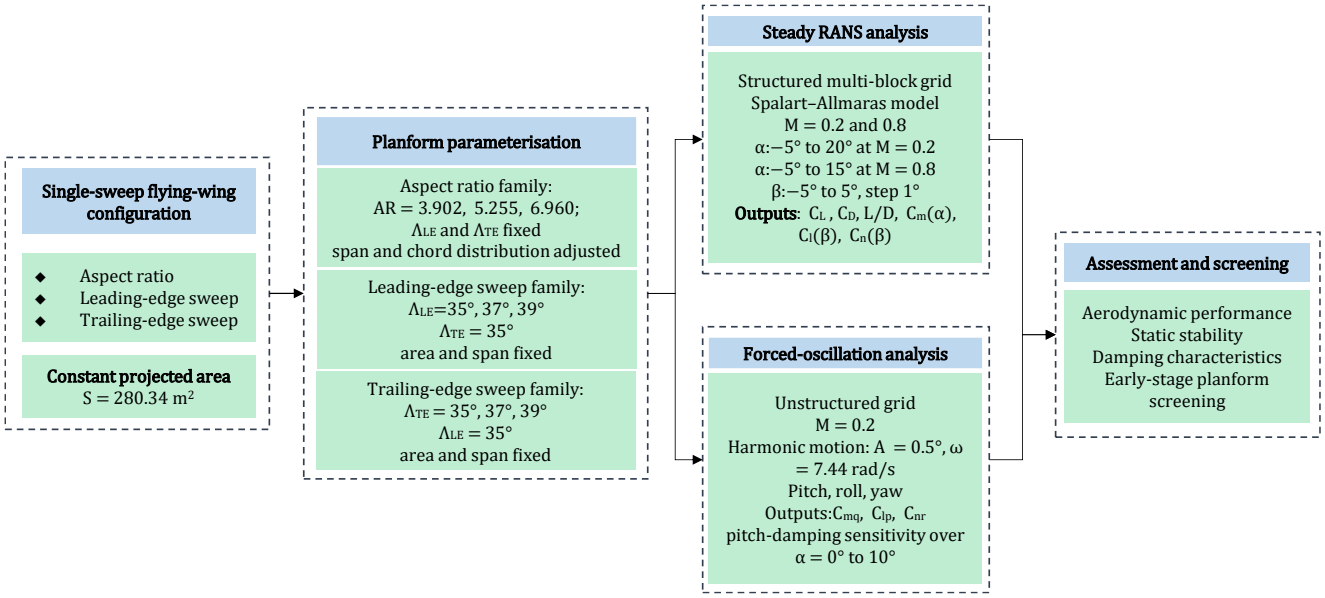


Figure 2 - Computational workflow for planform-parameter evaluation and early-stage flying-wing configuration screening.

3 Results and discussion

3.1 Aerodynamic performance (L/D)

Figure 3 and Figure 4 compare the lift-to-drag ratio L/D as a function of angle of attack for the three planform-parameter families at M = 0.2 and M = 0.8, respectively. For early-stage configuration screening, the discussion focuses on the peak L/D, the corresponding angle-of-attack range, and the behaviour of the L/D curve around and beyond the peak.

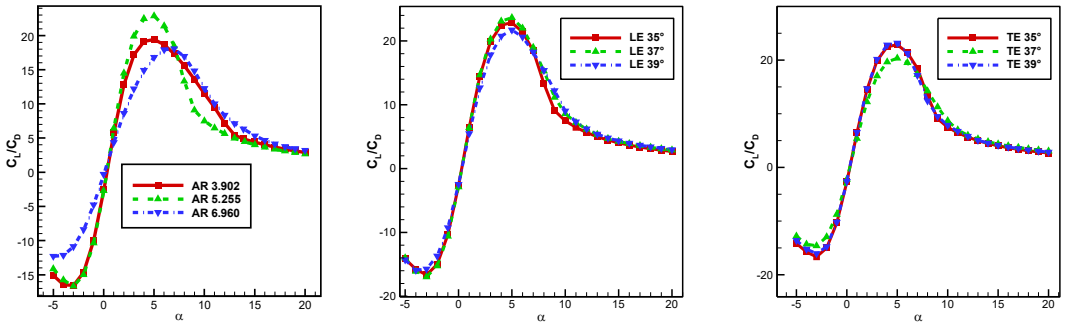


Figure 3 - Lift-to-drag ratio versus angle of attack at M = 0.2 for AR, Λ_{LE} and Λ_{TE} families.

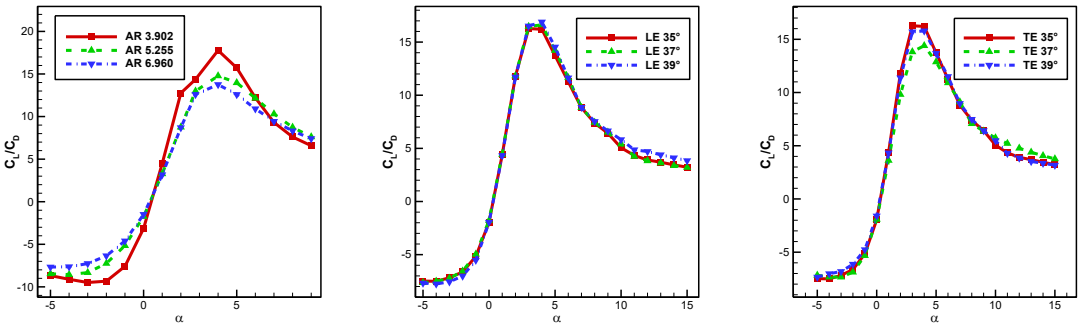


Figure 4 - Lift-to-drag ratio versus angle of attack at M = 0.8 for AR, Λ_{LE} and Λ_{TE} families.

Overall, the three planform parameters lead to moderate changes in the global shape of the L/D curves. At M = 0.2, the peak L/D generally occurs within $\alpha \approx$ 4°– 6°. At M = 0.8, the post-peak decrease becomes more pronounced, indicating that compressibility-related effects impose a stronger constraint on the usable angle-of-attack range. Although the peak values are relatively close among some variants, the parameter changes affect the peak-region width and the high-α decay rate, both of which are relevant to early-stage planform selection.

For the aspect-ratio family, the influence of AR on L/D is not strictly monotonic under the present constant-area constraint. Although increasing AR can reduce the induced-drag component in principle, it also changes the spanwise loading, chord-length distribution, wetted-area contribution and local viscous characteristics of the flying-wing planform. As a result, the highest-AR case does not necessarily produce the highest peak L/D in Figure 3. The present results therefore indicate that AR is an important parameter for aerodynamic-efficiency screening, but its effect should be interpreted together with the associated changes in loading distribution, trim requirement and static stability.

For the leading-edge sweep family, the L/D curves remain relatively close at M = 0.2, suggesting that Λ_{LE} is not the dominant factor governing low-speed aerodynamic efficiency within the tested range. At M = 0.8, the differences among the Λ_{LE} variants become more visible, especially in the peak region and the post-peak decay. This indicates that leading-edge sweep plays a more important role under the higher-Mach-number condition, where compressibility effects become more relevant.

For the trailing-edge sweep family, the influence of Λ_{TE} on L/D is limited near small angles of attack but becomes more evident at moderate to high angles of attack. Compared with the aspect-ratio family, the trailing-edge sweep variation does not act as a simple aerodynamic-efficiency parameter. Instead, its influence should be interpreted together with the static-stability and damping-derivative results,

because Λ_{TE} affects the trade-off among aerodynamic efficiency, trim requirement, and damping characteristics.

3.2 Static stability

Static stability is assessed using the longitudinal pitching-moment curves and the lateral-directional moment responses to sideslip. For longitudinal static stability, the small-angle slope of the pitching-moment coefficient, $C_{m\alpha}$, is used as the main indicator, where a negative slope corresponds to a restoring pitching-moment tendency. For lateral-directional static stability, the near-zero-sideslip trends of C_l and C_n are examined to evaluate the rolling- and yawing-moment responses.

Compared with the relatively moderate changes observed in the L/D curves, the planform parameters produce more evident variations in the pitching-moment behaviour. Figure 5 and Figure 8 show the pitching-moment coefficient versus angle-of-attack curves at M = 0.2 and M = 0.8, respectively. Figure 6 and Figure 7 present the lateral-directional static-stability trends at M = 0.2, while Figure 9 and Figure 10 show the corresponding results at M = 0.8. These results indicate that the stability-related effects of planform variation should be evaluated together with aerodynamic efficiency during early-stage configuration screening.

The sign change of $C_{m\alpha}$ observed in the sweep-angle cases can be interpreted from the redistribution of the incremental lift with angle of attack. When the sweep angle is changed, the planform geometry modifies the local chord distribution, spanwise loading pattern and effective moment arm of the lift increment. For the present moment reference point, this redistribution can shift the effective centre of the incremental lift rearwards relative to the reference point, thereby producing a stronger nose-down pitching-moment increment as α increases. Consequently, the pitching-moment slope may change from weakly positive to negative for the selected sweep-angle cases. This behaviour is therefore considered physically reasonable within the present planform family and reference-point definition, although its magnitude should be interpreted as configuration-specific rather than as a universal sweep-angle trend.

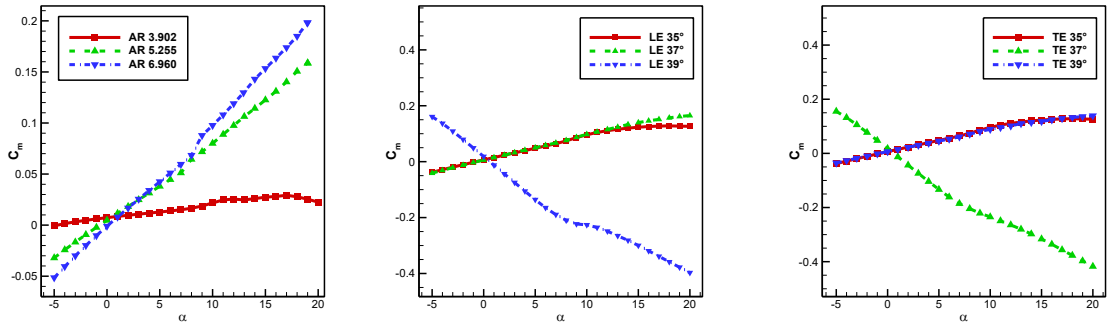


Figure 5 - Pitching-moment coefficient versus angle of attack at M = 0.2 for AR, Λ_{LE} and Λ_{TE} families.

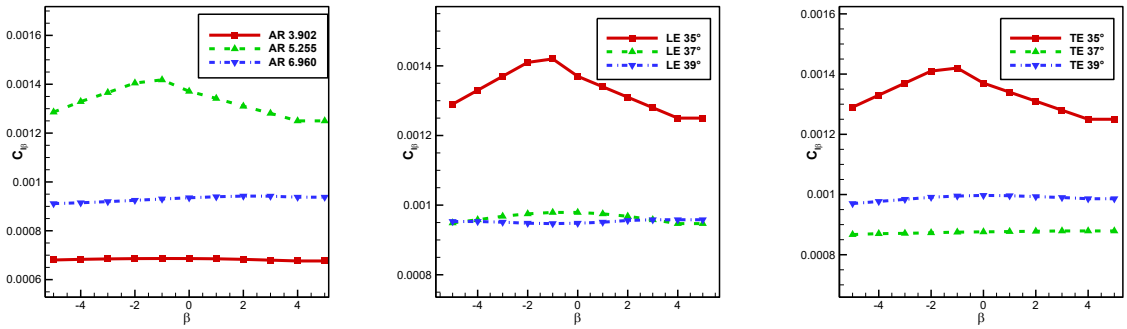


Figure 6 - Rolling-moment coefficient response versus sideslip at M = 0.2.

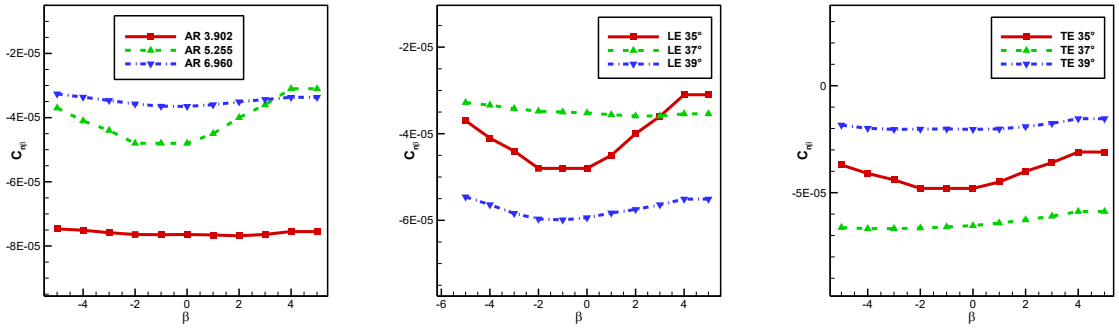


Figure 7 - Yawing-moment coefficient response versus sideslip at M = 0.2.

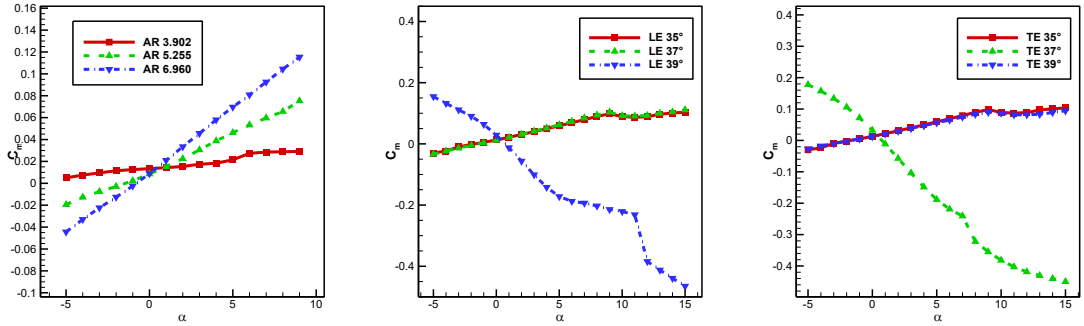


Figure 8 - Pitching-moment coefficient versus angle of attack at M = 0.8 for AR, Λ_{LE} and Λ_{TE} familie s.

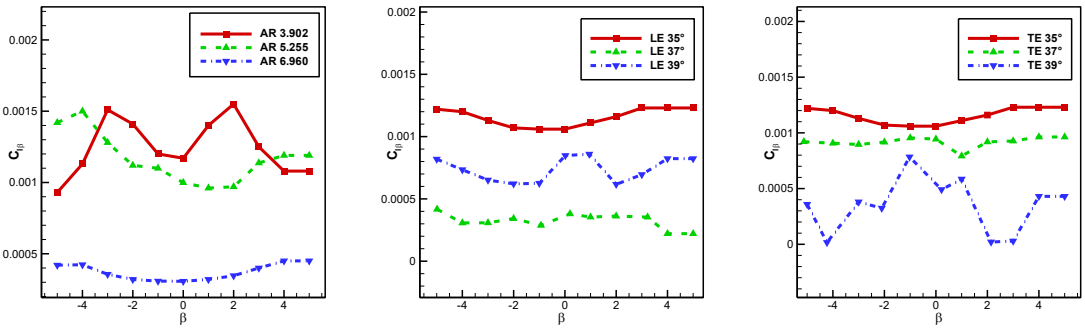


Figure 9 - Rolling-moment coefficient response versus sideslip at M = 0.8.

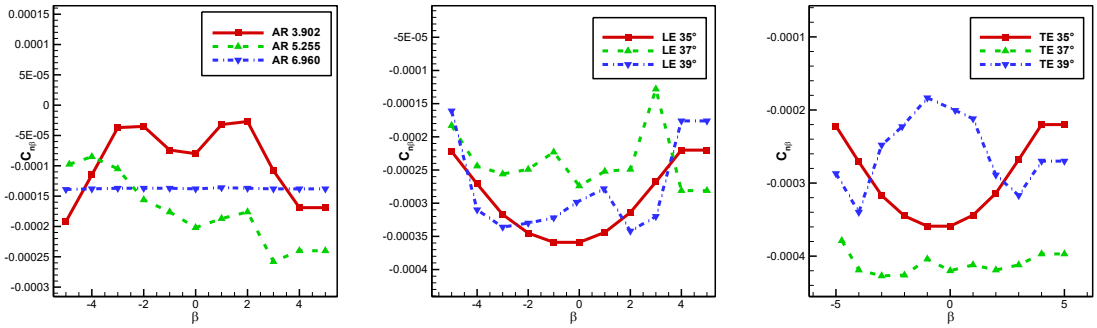


Figure 10 - Yawing-moment coefficient response versus sideslip at M = 0.8.

For the aspect-ratio family, increasing AR from 3.902 to 6.960 generally makes the linear-range $C_{m\alpha}$ slope more positive, indicating a reduction in longitudinal static stability among the tested cases. The

pitching-moment magnitude also increases with angle of attack, implying a higher trim or control-authority requirement. Therefore, although a higher aspect ratio can improve aerodynamic efficiency, its benefit should be constrained by the associated longitudinal stability and trim penalties.

For the leading-edge sweep family, the cases with Λ_{LE} = 35° and 37° show similar longitudinal pitching-moment trends, with a weakly unstable tendency in the small-angle range. When Λ_{LE} is increased to 39°, the pitching-moment slope becomes more favourable and remains negative over a wider angle-of-attack range. This suggests that, for the present reference point and planform family, increasing the leading-edge sweep to ΛLE = 39° shifts the pitching-moment trend towards a stronger restoring tendency within the tested range. However, its influence on lateral-directional stability should still be interpreted together with the roll- and yaw-moment responses shown in Figure 6, Figure 7, Figure 9 and Figure 10.

For the trailing-edge sweep family, Λ_{TE} = 35° and 39° generally lead to a positive $C_{m\alpha}$ in the small-angle range, whereas Λ_{TE} = 37° produces a negative pitching-moment slope at both Mach numbers. Among the tested cases, this intermediate trailing-edge sweep therefore provides the most favourable longitudinal static-stability tendency, indicating that the effect of trailing-edge sweep is not simply monotonic but depends on the resulting chord distribution and moment-arm variation. Nevertheless, the selection of Λ_{TE} should not be based on longitudinal stability alone, because trailing-edge sweep also affects aerodynamic efficiency and damping characteristics, as discussed in Sections 3.1 and 3.3.

3.3 Dynamic stability (damping derivatives)

The static-stability indicators discussed in Section 3.2 describe the initial restoring tendency under small perturbations, but they do not quantify the aerodynamic damping associated with rotational motion. Therefore, selected damping derivatives are further examined to assess the low-speed dynamic-stability characteristics of the flying-wing variants. In the present study, the analysis focuses on the pitch, roll, and yaw damping derivatives, namely C_{mq}, C_{lp}, and C_{nr}.

Because forced-oscillation simulations require multiple unsteady cycles and are considerably more expensive than the steady computations, the dynamic-stability analysis is less extensive than the static-stability assessment. The damping derivatives are evaluated only at M = 0.2. Figure 11 compares the three principal damping derivatives at α = 0° and β = 0° for the three planform-parameter families. Figure 12 further presents the variation of the pitch damping derivative over α = 0° to 10°.

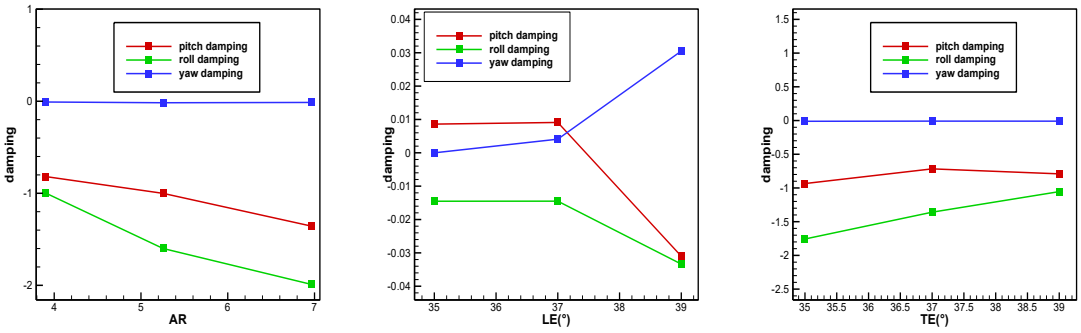


Figure 11 - Damping derivatives at M = 0.2, α = 0°, β = 0° for AR, Λ_{LE} and Λ_{TE} families.

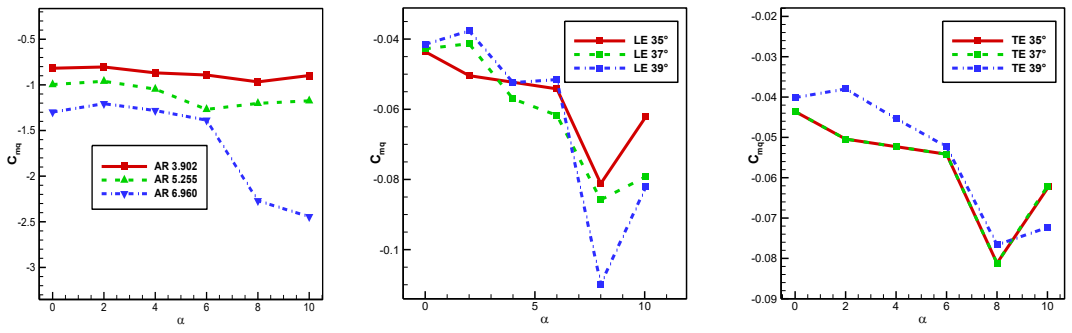


Figure 12 - Pitch damping derivative C_{mq} versus α (0°-10°) at M = 0.2.

As shown in Figure 11, the three planform parameters exhibit different sensitivities in the damping derivatives. For the aspect-ratio family, increasing AR generally increases the magnitude of pitch and roll damping, indicating a stronger damping response in pitch and roll at the low-speed reference condition. The yaw damping derivative remains smaller in magnitude and shows weaker monotonicity. This suggests that the effect of AR is more evident in the pitch and roll damping channels than in the yaw damping response.

For the leading-edge sweep family, the variation in yaw damping is more noticeable than that in the other two damping derivatives. This indicates that Λ_{LE} has a stronger influence on the lateral-directional unsteady moment response, especially in yaw. By contrast, the pitch and roll damping derivatives are less sensitive to Λ_{LE} within the tested range.

For the trailing-edge sweep family, the pitch and roll damping derivatives show the strongest sensitivity among the three parameter families. This result indicates that Λ_{TE} plays an important role in shaping the unsteady moment response in pitch and roll. Combined with the static-stability results in Section 3.2, this also indicates that trailing-edge sweep should be treated as a key parameter in the stability-related stage of planform screening.

Figure 12 shows that the pitch damping derivative becomes more sensitive to angle of attack as α increases. In particular, the variation becomes more evident around the mid-angle-of-attack range. This suggests that evaluating damping only at α = 0° may be insufficient for planform down-selection, especially when the configuration is expected to operate over a wider angle-of-attack range. Therefore, the damping margin at moderate angles of attack should be checked as a complementary consideration after aerodynamic-efficiency and static-stability screening.

4 Conclusions

This study examined the effects of aspect ratio, leading-edge sweep and trailing-edge sweep on the aerodynamic and stability characteristics of a single-sweep flying-wing configuration under a constant projected-area constraint. Steady RANS computations were used to evaluate the aerodynamic-efficiency and static-stability trends at M = 0.2 and M = 0.8, while selected forced-oscillation simulations were conducted at M = 0.2 to assess the damping-derivative response.

The results show that the three planform parameters affect aerodynamic efficiency in different ways. At M = 0.2, the peak L/D generally occurs within α $\approx$ 4°-6°, whereas the post-peak degradation becomes more pronounced at M = 0.8. The aspect-ratio variation changes both the peak level and the width of the near-peak region, but its influence on L/D is not strictly monotonic under the present constant-area constraint. The influence of leading-edge sweep is relatively weak at low speed but becomes more visible at the higher Mach number. Trailing-edge sweep has a limited effect near small angles of attack, but its influence becomes more evident as the angle of attack increases.

The static-stability results indicate that aerodynamic-efficiency trends alone are insufficient for planform down-selection. Increasing aspect ratio tends to reduce longitudinal static stability in the tested cases, while its aerodynamic-efficiency effect is not monotonic under the present constant-area constraint. Increasing the leading-edge sweep to ΛLE = 39° improves the longitudinal restoring tendency within the tested range, while the intermediate trailing-edge sweep, ΛTE = 37°, gives the most favourable longitudinal static-stability behaviour among the three trailing-edge sweep cases. These findings suggest that trim and static-stability constraints should be considered together with aerodynamic performance in the early design stage.

The damping-derivative results further show that different planform parameters dominate different dynamic-stability channels at M = 0.2. Aspect ratio mainly affects pitch and roll damping, leading-edge sweep has a more noticeable effect on yaw damping, and trailing-edge sweep shows the strongest sensitivity in pitch and roll damping. The pitch damping derivative also becomes more sensitive to angle of attack in the moderate-angle range, suggesting that damping verification at α = 0° alone may be insufficient for configuration screening.

Based on these findings, a progressive planform-screening strategy is recommended for this class of flying-wing configurations. Aspect ratio should be used to define candidate aerodynamic layouts together with stability constraints, rather than being treated as a purely beneficial efficiency parameter. Sweep parameters should then be evaluated under trim and static-stability constraints, and trailing-edge sweep should receive particular attention in the damping-derivative verification stage. The present dynamic-stability assessment is limited to selected forced-oscillation cases at M = 0.2, and future work should extend the analysis to broader Mach-number and angle-of-attack ranges and incorporate control-surface effects.

5 Contact Author Email Address

Huan Zhao: huanzhao@nwpu.edu.cn

6 Copyright Statement

The authors confirm that they, and/or their company or organization, hold copyright on all of the original material included in this paper. The authors also confirm that they have obtained permission, from the copyright holder of any third party material included in this paper, to publish it as part of their paper. The authors confirm that they give permission, or have obtained permission from the copyright holder of this paper, for the publication and distribution of this paper as part of the ICAS proceedings or as individual off-prints from the proceedings.

7 Acknowledgement

This work was supported by the National Natural Science Foundation of China (NSFC) under Grant No. 52572420 and by the Foundation of the National Key Laboratory of Aircraft Configuration Design under Grant No. JBGS-202502. This support is gratefully acknowledged.

References

[1] Mader, C. A., and Martins, J. R. R. A., “Stability-Constrained Aerodynamic Shape Optimization of Flying Wings,” Journal of Aircraft, Vol. 50, No. 5, 2013, pp. 1431–1449. DOI: 10.2514/1.C031956.

[2] Lyu, Z., and Martins, J. R. R. A., “Aerodynamic Design Optimization Studies of a Blended-Wing-Body Aircraft,” Journal of Aircraft, Vol. 51, No. 5, 2014, pp. 1604–1617. DOI: 10.2514/1.C032491.

[3] Park, J., Choi, J.-Y., Jo, Y., and Choi, S., “Stability and Control of Tailless Aircraft Using Variable-Fidelity Aerodynamic Analysis,” Journal of Aircraft, Vol. 54, No. 6, 2017, pp. 2148–2164. DOI: 10.2514/1.C034052.

[4] Donlan, C. J., “An Interim Report on the Stability and Control of Tailless Airplanes,” NACA Report No. 796, 1944. (NASA NTRS PDF available).

[5] Etkin, B., and Reid, L. D., Dynamics of Flight: Stability and Control, 3rd ed., John Wiley & Sons, 1995. ISBN: 978-0471034186.

[6] Da Ronch, A., Vallespin, D., Ghoreyshi, M., and Badcock, K. J., “Computation of Dynamic Derivatives Using CFD,” 28th AIAA Applied Aerodynamics Conference, 2010. AIAA Paper 2010-4817. DOI: 10.2514/6.2010-4817.

[7] Da Ronch, A., Vallespin, D., Ghoreyshi, M., and Badcock, K. J., “Evaluation of Dynamic Derivatives Using Computational Fluid Dynamics,” AIAA Journal, Vol. 50, No. 2, 2012, pp. 470–484. DOI: 10.2514/1.J051304.

[8] Vicroy, D. D., A Guide to Forced Oscillation Data Processing and Analysis, NASA/TP–20210023569, June 2023.

[9] Nguyen, N., Xiong, J., and Su, W., “CFD-Based Frequency Domain Method for Dynamic Stability Derivative Estimation with Application to Transonic Truss-Braced Wing,” NASA NTRS Document ID 20220008236, 2022.

[10] Krist, S. L., Biedron, R. T., and Rumsey, C. L., “CFL3D User’s Manual (Version 5.0),” NASA/TM-1998-208444, June 1998.